Journal of Magnetic Resonance **154,** 261–268 (2002)
doi:10.1006/jmre.2001.2474, available online at http://www.idealibrary.com on IDEAL®

T_1–T_2 Correlation Spectra Obtained Using a Fast Two-Dimensional Laplace Inversion

Y.-Q. Song,[1] L. Venkataramanan, M. D. Hürlimann, M. Flaum, P. Frulla, and C. Straley

Schlumberger–Doll Research, Old Quarry Road, Ridgefield, Connecticut 06877

Received July 11, 2001; revised October 30, 2001; published online January 16, 2002

Spin relaxation is a sensitive probe of molecular structure and dynamics. Correlation of relaxation time constants, such as T_1 and T_2, conceptually similar to the conventional multidimensional spectroscopy, have been difficult to determine primarily due to the absense of an efficient multidimensional Laplace inversion program. We demonstrate the use of a novel computer algorithm for fast two-dimensional inverse Laplace transformation to obtain T_1–T_2 correlation functions. The algorithm efficiently performs a least-squares fit on two-dimensional data with a nonnegativity constraint. We use a regularization method to find a balance between the residual fitting errors and the known noise amplitude, thus producing a result that is found to be stable in the presence of noise. This algorithm can be extended to include functional forms other than exponential kernels. We demonstrate the performance of the algorithm at different signal-to-noise ratios and with different T_1–T_2 spectral characteristics using several brine-saturated rock samples.

Key Words: **T_1, T_2, T_1–T_2 correlation; Laplace inversion.**

I. INTRODUCTION

Multidimensional correlations have been the central concept in modern NMR spectroscopy for studies of molecular structures and dynamics (*1*). The technical advances in computer hardware and efficient algorithms (such as fast Fourier transform) have helped to make the handling of multidimensional data a routine task. Relaxation properties, such as T_1 and T_2, may also be used to identify molecular species and to study their dynamics. The multidimensional correlation functions of such parameters are of great interest (*2, 3*). Experiments to obtain such correlation functions are entirely analogous to the multidimensional NMR spectroscopy methods in that the signal is measured as a function of two or more independent variables (such as times) allowing the spin system to evolve under different relaxation mechanisms. However, the analysis of such relaxation correlation data requires a multidimensional inverse Laplace transform. The difficulty in performing this analysis (*3*) has greatly impeded the application of this method.

[1] To whom correspondence should be addressed. E-mail: song@ridgefield.sdr.slb.com.

We will illustrate this general issue using the T_1–T_2 correlation experiment as an example. The data can be acquired using a conventional inversion–recovery experiment detected by a CPMG pulse train (*2, 3*). This pulse sequence is shown in Fig. 1. The recovery time, τ_1, and the echo time τ_2, are two independent variables and the acquired data can be written as a two-dimensional array, $M(\tau_1, \tau_2)$. Over the time period τ_1, the spin magnetization decays along the z axis, a T_1 process. However, during τ_2, the decay is due to T_2 . This signal relates to the probability density of T_1 and T_2 via an integral (*3*)

$$M(\tau_1, \tau_2) = \int\int (1 - 2e^{-\tau_1/T_1})\, e^{-\tau_2/T_2} \mathcal{F}(T_1, T_2)\, dT_1 dT_2 + E(\tau_1, \tau_2), \quad [1]$$

where $E(\tau_1, \tau_2)$ is the experimental noise. The function $\mathcal{F}(T_1, T_2)$ corresponds to the probability density of molecules with relaxation times of T_1, T_2. Therefore, $\mathcal{F}(T_1, T_2) \geq 0$ for all T_1 and T_2 . The part of the integrand $(1-2e^{-\tau_1/T_1})e^{-\tau_2/T_2}$ that relates $T_{1,2}$ and $\tau_{1,2}$ respectively is called the kernel.

One specific application of the T_1–T_2 correlation spectrum is to obtain the T_1/T_2 ratio for the study of the molecular mechanisms of surface relaxation, particularly in porous materials (*4, 5*). In a previous study on water saturated sedimentary rocks (*6*), separate measurements of T_1 and T_2 relaxation were made and an average T_1/T_2 ratio was extracted from a comparison of the corresponding T_1 and T_2 distributions. This simple method works only when the T_1 and T_2 distributions are similar. On the other hand, if one can measure $\mathcal{F}(T_1, T_2)$, the average T_1/T_2 ratio can be calculated by integration. What is more important is that $\mathcal{F}$ will enable us to identify different molecular species with distinct T_1/T_2 ratios. This quantity is of great interest in the study of tissues in organisms (*2, 3*).

Equation [1] is an example of a broad class of Fredholm integrals of the first kind that is frequently encountered in image restoration and other applications (*7*). For example, in image processing, the kernel may correspond to a blurring mechanism. It is well known that inverting Fredholm integrals with smooth kernels is an ill-conditioned problem in the sense that a small change in M will cause a large change in $\mathcal{F}$. The solution for

1090-7807/02 $35.00

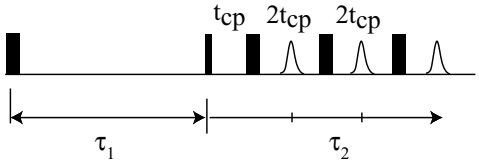

FIG. 1. The pulse sequence used for the T_1–T_2 correlation experiments. All pulses are 180° pulses except for the second pulse being 90°. Echo signals were detected at midway between two adjacent 180° pulses. CPMG signals were collected for typically 30 values of τ_1. The phases used were, for the first 180° pulse: 0, 180; for the 90° pulse: 0, 0, 180, 180; and for the 180° pulses in the CPMG train: 90. The acquisition phase followed that of the 90° pulse.

Fredholm integrals is often obtained with certain assumptions about the character of E and $\mathcal{F}$. For example, $\mathcal{F}$ is assumed to be smooth.

There are several algorithms for inverse Laplace transform in one dimension (*8–10*). However, the straightforward extension of such algorithms to two-dimensions makes an enormous demand on computer memory and speed and has been accomplished only on a Cray (*3*). It would be very desirable to develop a method that can be used on desktop computers.

Our previous publication (*11*) described an efficient algorithm to solve this problem and we implemented it on a SUN Sparc workstation. The algorithm was used to examine several simulated data sets with different features in the T_1–T_2 distribution. It was demonstrated that this algorithm performed well and that the results for $\mathcal{F}$ were stable against different realizations of noise. In this paper, we will first review the essential aspects of the algorithm and then focus on the use of the algorithm to analyze experimental data. This is an important test of the algorithm because of the potential systematic noise present in experimental data.

II. BRIEF REVIEW OF THE ALGORITHM

We now summarize the mathematical model considered here and in Ref. (*11*). The data M relates to the kernel function through a Fredholm integral of the first kind

$$M(\tau_1, \tau_2) = \int\int k_1(x, \tau_1) k_2(y, \tau_2) \mathcal{F}(x, y)\, dx dy + E(\tau_1, \tau_2), \quad [2]$$

where $E(\tau_1, \tau_2)$ denotes the experimental noise that is assumed to be additive, zero mean, white Gaussian noise. The objective is to estimate $\mathcal{F}$ subject to the nonnegativity constraint: $\mathcal{F}(x, y) \geq 0$ for all x and y. Equation [1] is a special case of Eq. [2]. Because of the similarity with conventional two-dimensional spectroscopy, we shall call $\mathcal{F}(x, y)$ the spectrum of x and y.

Equation [2] can be approximated by a discretized matrix form

$$M = K_1 F K_2' + E, \quad [3]$$

where matrices K_1, K_2, and F are discretized version of k_1, k_2, and $\mathcal{F}$ respectively, and with dimensions $N_1 \times N_x$, $N_2 \times N_y$, and $N_x \times N_y$. The data matrix M is often large and typically highly redundant.

Inversion of Eq. [3] is in general ill-conditioned in the sense that a small change in M may result in a large change in $\mathcal{F}$. The general strategies to solve this problem have been discussed extensively in the mathematical literature (*12*). Numerical recipes (*13*) and other NMR literature (*9, 10, 14*) are a good introduction. One technique uses regularization and obtains a fit to the data through minimization of the expression

$$\|M - K_1 F K_2'\|^2 + \alpha \|F\|^2, \quad [4]$$

where $\|.\|$ denotes the Frobenius norm of a matrix. The first term measures the difference between the data and the fit. The second term is a Tikhonov regularization and its amplitude is controlled by the parameter α. The regularization term is a measure of the desired smoothness in F and makes the inversion less ill-conditioned. However, it may cause a bias to the result. When α is chosen such that the two terms are comparable, the bias is minimized and the result is stable in the presense of noise. When α is smaller than the optimal value, the result becomes unstable.

In order to accelerate the minimization of Eq. [4] we exploit the separable kernel structure for an efficient data compression using independent singular value decompositions (SVD) of K_1 and K_2,

$$K_1 = U_1 \Sigma_1 V_1', \quad [5]$$

where Σ_1 is a diagonal matrix with singular values in a descending order, U_1 and V_1 are unitary matrices. Σ_1 is the property of K_1 and the singular values typically decay quickly. We limit our algorithm to the subspace spanned by the typically 8–10 largest singular values for each of K_1 and K_2, respectively. This results in products of the singular values of K_1 and K_2 ranging over three orders of magnitude. Such a subspace is adequate for the limited signal-to-noise (S/N) ratio of experimental data. Using SVD of K_1 and K_2, Eq. [4] can be rewritten in an identical structure but with the compressed data $\tilde{M} = U_1' M U_2$ and kernels of much smaller dimensions, thus avoiding large memory requirements. Often, a total of about 50–100 variables are used in the subsequent optimization step.

In contrast without compression, if K_1 and K_2 were to be combined into one matrix K, Eq. [3] is restated in a one-dimensional form,

$$\mathbf{M} = K\mathbf{F} + \mathbf{E}, \quad [6]$$

where $\mathbf{M}$, $\mathbf{F}$, and $\mathbf{E}$ are vectors obtained by lexicographically ordering matrices M, F, and E, respectively. The dimension of K for the above equation would be $(N_1 N_2) \times (N_x N_y)$. For a typical T_1–T_2 correlation experiment with $N_1 = 4000$, $N_2 = 30$, $N_x = 100$, and $N_y = 100$, the dimension of matrix K is therefore

1.2×10^5 by 10^4. Thus, performing SVD of K would require large amount of memory and CPU time, and is impractical. For example, English *et al*. (*3*) required a CRAY supercomputer to estimate a coarsely discretized density function ($N_x = N_y = 35$) even from a small ($N_1 = 50$, $N_2 = 50$) data set.

In Ref. (*11*), we solved this particular class of the two-dimensional Fredholm integrals, such as Eq. [3], in three main steps. In the first step, the data is compressed using SVDs of the kernels, exploiting the tensor-production structure of the kernel, as discussed previously. In the second step, the constrained optimization problem is transformed to an unconstrained optimization problem in typically a lower dimensional space. This step uses a method adapted from the Butler, Reed, and Dawson (BRD) algorithm (*15*). The dimensionality of the vector space for the unconstrained optimization problem equals the size of the compressed data. In the third step, the optimal amplitude of the regularization term (α) was chosen by BRD (*15*) or S-curve method (*10*). The essence of both of these methods for choosing α is to find the most stable solution with the fit error $\|M - K_1 F K_2'\|^2$ similar to the known noise variance.

III. EXPERIMENTAL

T_1–T_2 correlation experiments were performed on bulk water and several water saturated rock samples using a Maran NMR spectrometer (Resonance Instruments, UK) at a proton resonance frequency of 2 MHz. The pulse sequence is depicted in Fig. 1. Typically, data for 30 values of τ_1 and 4096 τ_2 points were acquired in a two-dimensional array. τ_1 varied logarithmically from 10 μs to a few seconds. The values of τ_2 were equally spaced with a step size of typically 200 μs. A minimum of 64 scans were accumulated to improve the signal-to-noise ratio. The wait time between successive scans was 5 s and a complete 2D experiment can take two or three hours.

Our sedimentary rock samples were 20 mm in diameter and 38 mm in length, saturated with brine. These rocks generally contain a wide range of pore sizes so that the T_1 and T_2 distributions are broad (*16*). The five samples used in this paper were chosen to illustrate several aspects of the inversion algorithm and they are listed in Table 1.

TABLE 1
A List of the Samples Used and Their T_1–T_2 Characteristics

Sample	S/N	Spectral characteristics
Indiana limestone	95	well extended distribution
Bulk water	79	good signal, a test of the resolution
Nugget sandstone	27	low porosity and poor signal, resulting in a broad distribution
Oolitic limestone	75	two water populations with different T_1/T_2 ratios
Berea 500 sandstone	72	relatively narrow main peak and an extended tail

Note. The signal-to-noise ratio (S/N) is defined as the maximum signal divided by the noise variance.

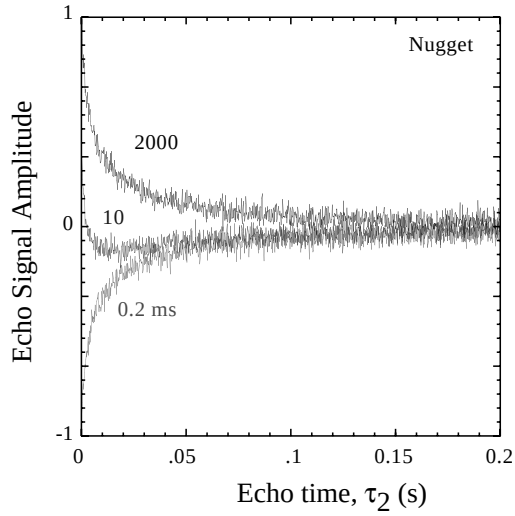

FIG. 2. Echo signals as a function of τ_1 and τ_2 for a Nugget sandstone obtained using the pulse sequence in Fig. 1. The decays are shown for τ_1 of 0.2, 10, and 2000 ms.

In Fig. 2, τ_2 decays for several values of τ_1 are shown for the Nugget sandstone sample. Existence of fast and slow relaxations is apparent from this graph. In particular, for $\tau_1 = 10$ ms, the fast relaxing components have already recovered substantially to give rise to a positive signal at early τ_2 while the long T_1 components remain negative.

IV. RESULTS

Figure 3 presents the T_1–T_2 spectrum for a sample of Indiana limestone showing a narrow ridge-like peak in the center of the graph. The range of T_1 and T_2 is approximately one and half orders of magnitude from 0.03 to 1 s, owing to its wide range of pore structures ranging from micrometer-size micropores to large vugs with millimeter dimension. It is remarkable that this ridge is closely parallel to the line for $T_1 = T_2$, meaning that all the water molecules in this rock essentially have an identical T_1/T_2 ratio. This is consistent with the notion that the relaxation in this rock is caused by a single surface mechanism throughout the sample and the distribution of T_1 and T_2 is due to the variation of local surface-to-volume ratio, or pore sizes (*5*, *16*).

From this 2D spectrum, one may obtain the 1D spectra of T_1 and T_2 by integrating the appropriate dimension. Such projected T_1 and T_2 distributions are compared with the corresponding T_1 and T_2 distributions obtained by conventional inversion recovery and CPMG sequence in Figs. 4A and 4B. Although the overall $T_{1,2}$ distributions are similar, those obtained from the 2D spectra contain more details. This suggests that 2D data might intrinsically have more information than the 1D data because more experiments are included.

Also, by integrating the 2D spectrum, we obtained the distribution of the T_1/T_2 ratio, Fig. 4C. The narrow distribution of

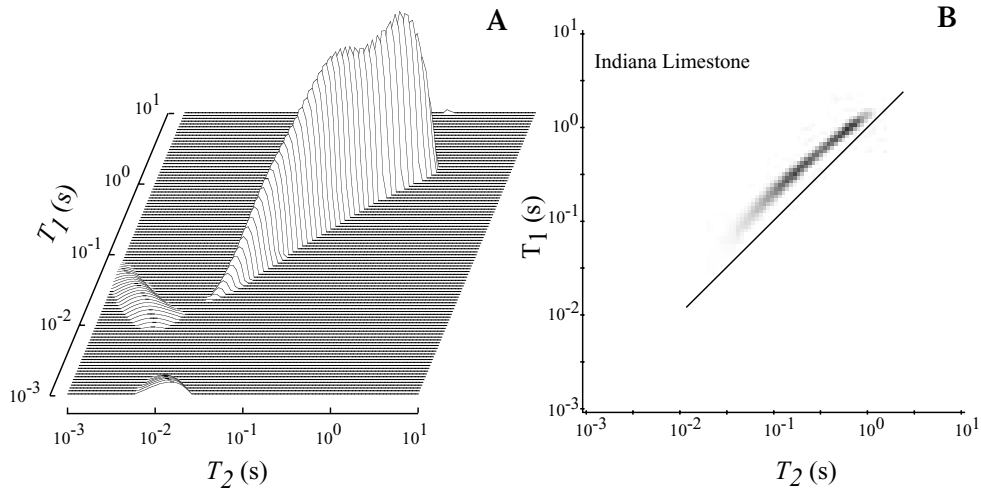

FIG. 3. The T_1–T_2 correlation spectrum for Indiana limestone in (A) a stack plot and (B) a density plot with a linear gray scale from zero to maximum amplitude. The line in (B) indicates $T_1 = T_2$.

the T_1/T_2 ratio is consistent with the narrow ridge in the 2D spectrum. Note that this method to measure T_1/T_2 ratio applies to arbitrary distributions of T_1 and T_2 .

For this rock, the ridge is rather narrow. It is important to examine whether this width is an intrinsic rock property or whether it is broadened by the inversion algorithm due to finite S/N ratio. For this purpose, we have measured the response of bulk water, doped with $NiCl_2$ to reduce the relaxation times. In this sample, we expect single exponential decays and it can be used to test the limit of the linewidth of the obtained T_1–T_2 spectrum due to finite signal-to-noise ratio.

Figure 5 shows the T_1–T_2 spectrum for bulk water, displaying a single peak at $T_1 \approx T_2 \approx 0.1$ s. The peak in the 2D spectrum centers at $T_2 = 0.091$ s and the base of the peak extends from $T_2 = 0.076$ to 0.11 s. At half the peak height, the width is 60% of that at the bottom. The width along the T_1 dimension is similar to that of the T_2 dimension, despite more τ_2 points. This result shows that with the given finite signal-to-noise ratio, it is mathematically impossible to distinguish decays with a single relaxation time constant from a narrow distribution of the relaxation time constant. Such dependence on signal-to-noise ratio has been demonstrated on the simulated data sets in our previous report (*11*). Compared to this, the T_2 width at half intensity for the Indiana limestone sample is approximately 2.6 times that for the bulk water sample. Although the total S/N ratio as defined in Table 1 is similar for the two samples, the Indiana limestone sample has a much broader spectrum than that of the water sample, thus the spectral amplitude at certain T_1 and T_2 is much lower than that of the water sample. Thus, it is possible that the broad linewidth of the Indiana limestone sample has contribution from the finite S/N ratio.

The effect of a reduced signal-to-noise is further illustrated with the Nugget sample of low porosity, 6% by volume. The spectrum (Fig. 6) shows a very extended ridge structure over two orders of magnitude. In addition, the width is much broader than for the water and Indiana limestone samples. The several low-amplitude bumps at the ends of the main ridge are likely to be residual artifacts due to noise on the spectrum.

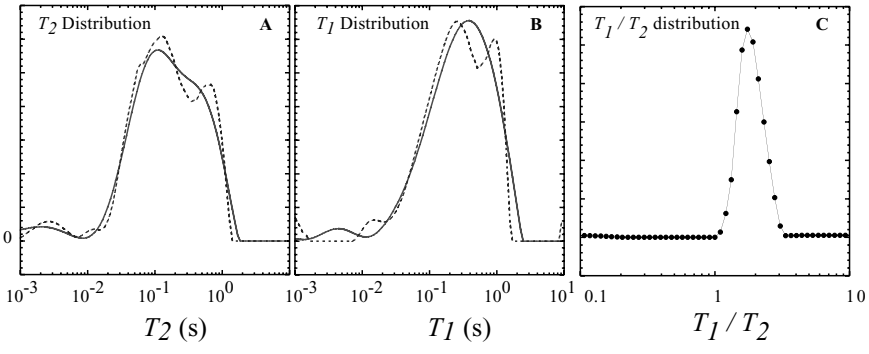

FIG. 4. (A, B) Comparison of T_1 and T_2 spectra for Indiana limestone, obtained by integrating the 2D spectra (dashed lines) and by conventional 1D inversion for the inversion–recovery and CPMG sequences (solid lines). (C) The distribution of T_1/T_2 ratio obtained by integrating the 2D spectrum.

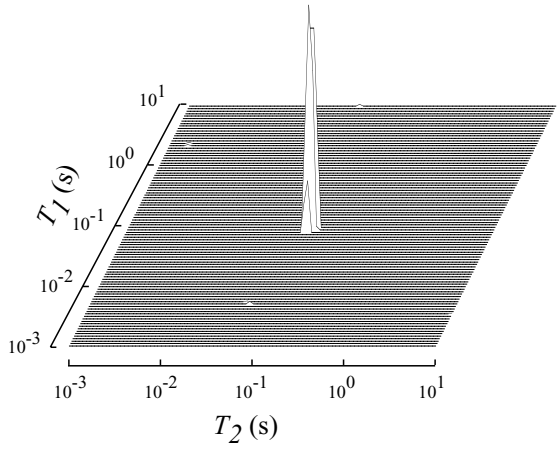

FIG. 5. The T_1–T_2 correlation spectrum for bulk water.

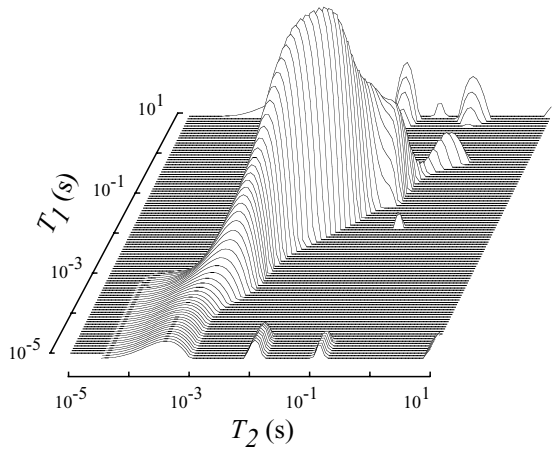

FIG. 6. The T_1–T_2 correlation spectrum for Nugget sandstone.

The spectrum of the oolitic limestone sample presents an interesting pattern, shown in a surface plot and a contour plot (Figs. 7A and 7B). Two separate peaks and a shoulder at $T_2 \approx 20$ ms are clearly observed. The two bumps along the edges of T_1 and T_2 axes are likely artifacts due to noise. The major peak at long T_1 and T_2 is approaching the line of $T_1 = T_2$ and in fact, $T_1/T_2 = 1.5$ at the top of the peak. In contrast, the peak at smaller T_1 and T_2 and one shoulder fall along the line of $T_1 = 4T_2$. The presence of separate peaks is a strong indication that there are two distinct environments for water in this rock. The components with small T_1 and T_2 are from water with its relaxation dominated by surface mechanism while the long T_1 and T_2 peak has a balance of contributions from surface and bulk. Since the measurement was performed at low frequency, 2 MHz, the internal field effect causing additional T_2 relaxation can be neglected. Assuming that the bulk relaxation contribution T_b is 2 s for both T_1 and T_2 , the observed relaxation rates are a sum of surface ($T^s_{1,2}$) and bulk contributions:

$$\frac{1}{T_{1,2}} = \frac{1}{T^s_{1,2}} + \frac{1}{T_b}. \qquad [7]$$

The solid line in Fig. 7 shows the possible values of T_1 and T_2 assuming $T^s_1/T^s_2 = 4.5$ and it is in good agreement with the

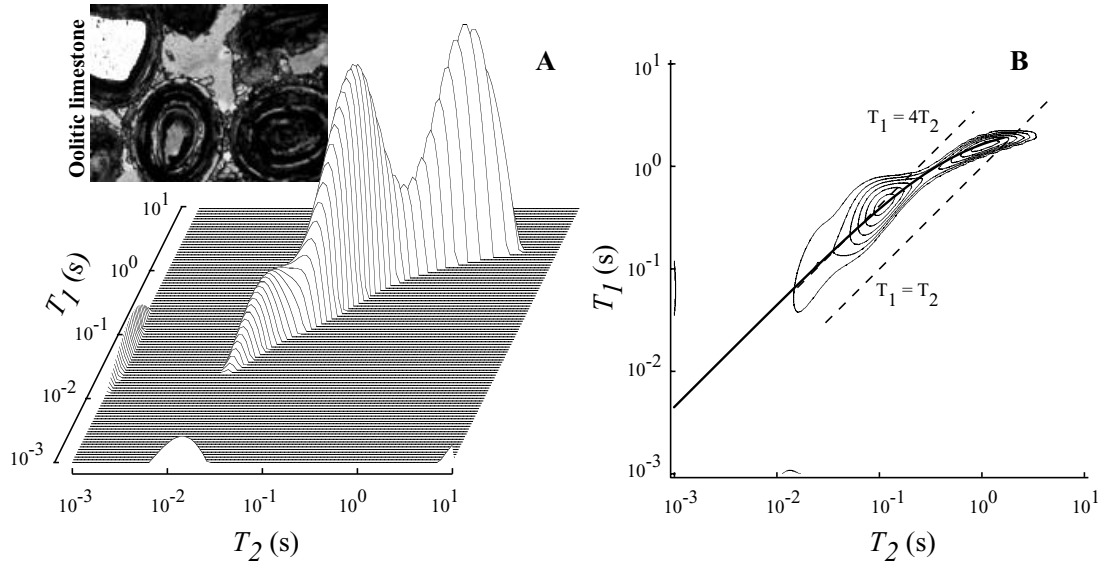

FIG. 7. The T_1–T_2 correlation spectrum for oolitic limestone. The dashed lines in (B) are for $T_1 = T_2$ and $T_1 = 4T_2$. The solid thick line is theoretical behavior of the sum of surface and bulk contributions to T_1 and T_2. The inset is a thin-section micrograph of the oolitic rock. The dark elliptical structures are grains of 200 micrometers and the gray regions are open pores.

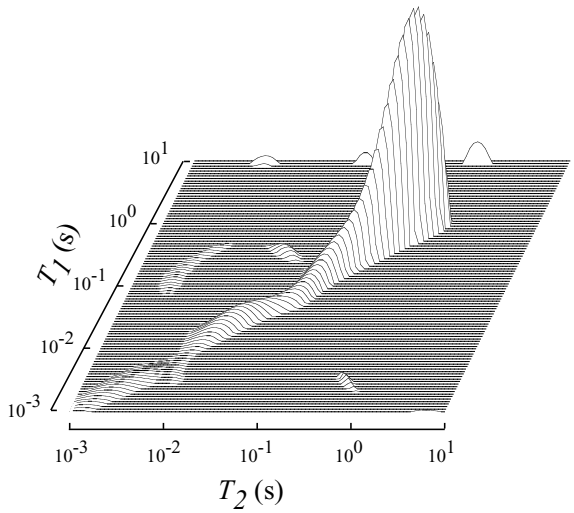

FIG. 8. T_1–T_2 correlation spectrum for Berea 500 sandstone.

observed data. This analysis confirms that the lower T_1/T_2 ratio for the long T_1 and T_2 component is the result of bulk contribution and the results are consistent with surface relaxation properties that are uniform throughout this rock.

The presence of two distinct pore environments is evident in the micrographs of 30-μm thin sections of the rock, shown in the inset of Fig. 7. The dark circular structures are porous grains (ooids), and inter-ooid pores are about 100 μm (the gray areas). The micropores inside the grains are apparently of much smaller sizes, thus they have a higher surface contribution to relaxation. From the result of a single T_1^s/T_2^s ratio for surface relaxation, one might infer that there is only one source of surface relaxation for both types of pores (intragranular and intergranular) because they are bound by the same solid material. We note that this value of T_1^s/T_2^s is considerably larger than is typically observed for sandstones and carbonate rocks (*6*).

The last sample is a Berea 500 rock from Berea, Kentucky. The T_1–T_2 spectrum, Fig. 8, shows a narrow ridge, similar to that of the Indiana limestone sample. However, the majority of the signal is concentrated at $T_1 = 0.6$ s and $T_2 = 0.5$ s, with a low amplitude tail at the regions of smaller T_1 and T_2 . This type of rock is often used as a model sample for petrophysical studies due to the homogeneity of its grain and pore sizes. Such homogeneity is the origin of the relatively narrow peak in the T_1–T_2 spectrum and is also reflected in the one-dimensional spectrum of T_1 or T_2 . From a signal processing point of view, this type of spectrum presents particular difficulties in assessing the errors of the spectral features (*9, 17*). Since the fit error is dominated by the main peak, the algorithm chooses α so that the main peak is stable. However, the lower amplitude tail extending to smaller T_1 and T_2 can still vary substantially due to noise. This instability is reflected in the irregular curving and shape of the tail deviating from the line of constant T_1/T_2. This is primarily the result of our use of a single regularization amplitude α.

V. DISCUSSIONS

A. Inversion Stability

Because the inverse Laplace transform is an ill-conditioned problem, the resulting spectrum can be strongly affected by noise. When the underlying problem can be formulated in a more restricted form using fewer parameters, it might be preferable to use a specialized fitting procedure. For a general purpose Laplace inversion of data with a finite S/N ratio, the resolution must be reduced to obtain a stable solution. In other words, there is not enough information in the data to determine the spectrum better than the stable spectrum.

In our algorithm, stability is obtained by using regularization and the procedure for the choice of the optimal regularization parameter, α. The principle for the choice of α is that the regularization term $\alpha \| F \|^2$ be comparable to the residual error. Typically, α is larger for data with lower signal-to-noise ratio, as demonstrated in our previous report (*11*). Here, we will further demonstrate the stability of the spectrum by using data with different realizations of noise. In Fig. 9, we show the inversion spectra of the Indiana limestone and Berea 500 samples from data sets that were obtained by adding white noise to the fits obtained from the spectra in Fig. 3 and Fig. 8, respectively. The amplitude of the added noise was the same as that in the original data. The BRD method was used to obtain the optimal values of

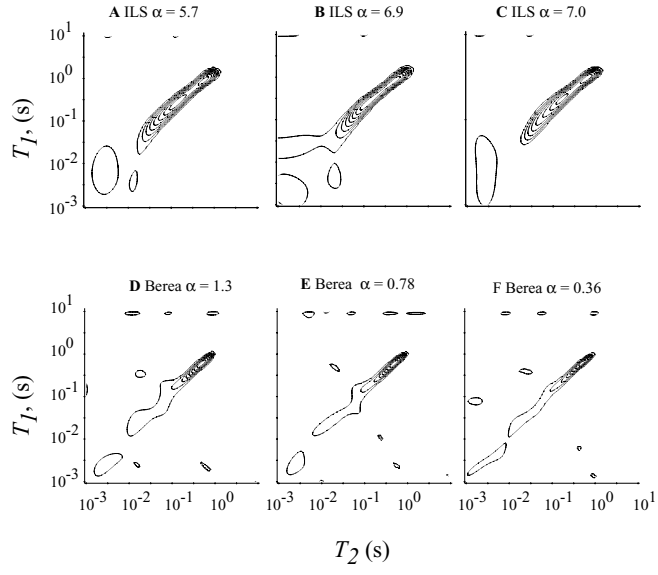

FIG. 9. The T_1–T_2 correlation spectra for the Indiana limestone (A, B, C) and Berea 500 samples (D, E, F) with three different noise realizations. The noises of the same amplitude as that in the original signals were created for each realization and added to the fits obtained from the spectra of Figs. 3 and 8. BRD method was used to find the optimal α for each inversion and its value is listed in the figures. For both samples, the main peaks appear to be very stable in all realizations, however, the low amplitude tails vary significantly at a few percent level. In all figures, nine equally spaced contours are used from 1 to 90% of the maximum amplitude.

α that are listed in the figures. We observe small changes of the optimal α for different noise realizations, but the main features of the spectra remain unchanged. The variation of the spectra appears only at an amplitude of a few percent of the maximum spectral amplitude.

B. Systematic Errors

Systematic errors can pose another difficulty for this algorithm since specific characteristics of the noise are assumed. For example, the noise, E, is assumed to be additive with a white frequency spectrum. Other types of noise, for example, the ringing noise from the rf pulses are not modeled by Eq. [2] and the algorithm will usually achieve a fit error χ larger than the variance of the white noise. This will also be true if the underlying spin dynamics cannot be described by our exponential kernels. In these cases, the effect of the systematic errors on the resulting spectrum depends sensitively on the exact nature of the errors.

An experimental problem often encountered is that the 180° pulse is inaccurate, so that the kernel changes to $[1-(2-\delta)e^{-\tau_1/T_1}]e^{-\tau_2/T_2}$. This problem can be resolved in two ways. The first method is to subtract from each CPMG decay data at certain τ_1 the CPMG decay at a τ_1 value that is at least 3–5 times the longest T_1, $M(\tau_1 \to \infty, \tau_2)$:

$$m \equiv M(\tau_1, \tau_2) - M(\infty, \tau_2). \qquad [8]$$

This changes the kernel correspondingly to $e^{-\tau_1/T_1}e^{-\tau_2/T_2}$. This method is preferable if one can measure $M(\infty, \tau_2)$ reliably. The second method is to add an extra constant column in K_1 for $T_1 = \infty$. Correspondingly, one column is added to F and the resulting amplitude of this column after the inversion will be related to the error of the inversion pulse angle.

Other types of systematic errors, such as pulse ringing and field inhomogeneities are dependent on the spectrometer hardware and are more difficult to model. One may inspect the original data for signs of such problems, in particular, by examining the imaginary channel after phase rotation. For all the data sets presented in this report, problems due to systematic errors were not apparent by inspecting the original data. However, the data for the Indiana limestone sample showed a problem in the convergence of α using the BRD method and the fit error at very small α was slightly larger than that estimated from random noise. This is likely due to some systematic errors with an amplitude comparable to that of the random noise. In this case, the optimal α was chosen by numerically calculating the fit error $\chi(\alpha)$ of the compressed data for a series of α and then finding α_{heel} by

$$\left.\frac{\partial \log \chi}{\partial \log \alpha}\right|_{\alpha_{heel}} = 0.1. \qquad [9]$$

This criterion chooses the optimal α at the heel of the $\chi(\alpha)$ curve (S-curve) which balances the residual fit error and the known noise variance (*10*, *18*). For simulated data without systematic errors, the BRD method always converges to an optimal α that is very close to the heel of the S-curve. We found that for the analysis of experimental data with small systematic errors, the S-curve method can be more robust than the BRD method. However, the calculation will generally take longer since inversion must be calculated for many values of α. For the Indiana limestone data, the BRD method did not converge and the optimal α was obtained by the S-curve method. For all other data sets, both BRD and S-curve methods were used and similar α were obtained.

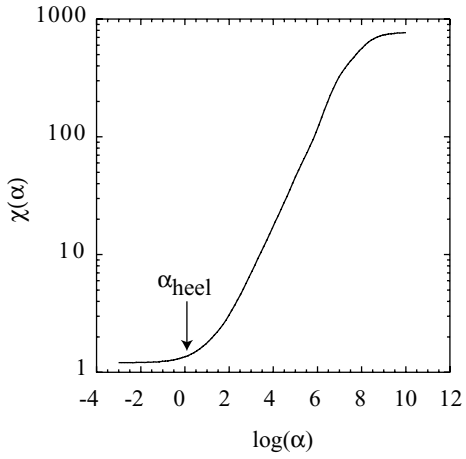

FIG. 10. The fit error $\chi(\alpha)$ for the Indiana limestone sample as a function of α, normalized by the noise standard deviation in the original data.

In Fig. 10, we show the fit error for the Indiana limestone sample as a function of α from 10^{-3} to 10^{10}, exhibiting the classic S-curve. According to Eq. [9] the optimal α is chosen to be 2.6, at the heel of the S-curve.

VI. CONCLUSIONS

We have demonstrated the use of a 2D Laplace inversion algorithm that is fast and efficient and can be implemented on desktop computers. The use of this algorithm will enable two-dimensional relaxation correlation spectroscopy for the study of molecular structures and dynamics. For example, it can be used to study exchange phenomena similar to NOESY, and to identify regions of the molecules with fast and slow dynamics from the measurement of T_1/T_2. Furthermore, the algorithm is not restricted to the exponential form of the kernel and can be easily extended to other functional forms.

ACKNOWLEDGMENTS

The authors acknowledge extensive discussion with W. Kenyon, S. Ryu, and C. Flaum.

REFERENCES

1. R. R. Ernst, G. Bodenhausen, and A. Wokaun, "Principles of Nuclear Magnetic Resonance in One and Two Dimensions," Oxford University Press, New York (1994).
2. H. Peemoeller, R. K. Shenoy, and M. M. Pintar, Two-dimensional NMR time evolution correlation spectroscopy in wet lysozyme, *J. Magn. Reson*. **45,** 193 (1981).
3. A. E. English, K. P. Whittall, M. L. G. Joy, and R. M. Henkelman, Quantitative two-dimensional time correlation relaxometry, *Magn. Reson. Medicine* **22,** 425 (1991).
4. P. Z. Wong, "Methods in the Physics of Porous Media," Academic Press, London (1999).
5. W. P. Halperin, F. D'Orazio, S. Bhattacharja, and J. C. Tarczon, *in* "Molecular Dynamics in Restricted Geometries" (J. Klafter and J. Drake, Eds.), Wiley, New York (1989).
6. R. L. Kleinberg, S. A. Farooqui, and M. A. Horsfield, T_1/T_2 ratio and frequency dependence of NMR relaxation in porous sedimentary rocks, *J. Colloid Interface Sci*. **158,** 195 (1993).
7. I. K. Abu-Shumays and L. D. Marinelli, A smoothing solution (unfolding) of a two dimensional density function from its spectrum, *J. Comp. Phys*. **7,** 219 (1971).
8. S. W. Provencher, CONTIN: A general purpose constrained regularization program for inverting noisy linear algebraic and integral equations, *Comput. Phys. Commun*. **27,** 229 (1982).
9. G. C. Borgia, R. J. S. Brown, and P. Fantazzini, Uniform-penalty inversion of multiexponential decay data, *J. Magn. Reson*. **132,** 65 (1998).
10. E. J. Fordham, A. Sezginer, and L. D. Hall, Imaging multiexponential relaxation in the (y, log T_1) plane, with application to clay filtration in rock cores, *J. Magn. Reson. Ser. A* **113,** 139 (1995).
11. L. Venkataramanan, Y.-Q. Song, and M. D. Hürlimann, Solving Fredholm integrals of the first kind with tensor product structure in 2 and 2.5 dimensions, *IEEE Trans.*, to appear.
12. C. L. Lawson and R. J. Hanson, "Solving Least Squares Problems," Prentice-Hall, Englewood Cliffs, NJ (1974).
13. W. H. Press, S. A. Teukolsky, W. T. Vetterling, and B. P. Flannery, "Numerical Recipes in C," Cambridge University Press, Cambridge (1997).
14. R. M. Kroeker and R. M. Henkelman, Analysis of biological NMR relaxation data with continuous distributions of relaxation times, *J. Magn. Reson*. **69,** 218 (1986).
15. J. P. Butler, J. A. Reeds, and S. V. Dawson, Estimating solutions of the first kind integral equations with nonnegative constraints and optimal smoothing, *SIAM J. Numer. Anal*. **18,** 381 (1981).
16. R. Kleinberg, *in* "Encyclopedia of Nuclear Magnetic Resonance" (D. M. Grant and R. K. Harris, Eds.), Wiley, New York (1995).
17. G. C. Borgia, R. J. S. Brown, and P. Fantazzini, Uniform-penalty inversion of multiexponential decay data, *J. Magn. Reson*. **147,** 273 (2000).
18. P. C. Hansen, Analysis of discrete ill-posed problems by means of the L-curve, *SIAM Rev*. **34,** 561 (1992).